Engineered Science
DOI: https://dx.doi.org/10.30919/es1469

Synthesis and Structural Studies of Perovskite-Ytterbium Manganate and Spinel-Cobalt Chromite Nanomaterials

Moldir Zhaisanbayeva,[1,*] Gennadiy S. Patrin,[2] Karima Seitbekova,[1] Marzhan Nurbekova[1] and Mukhametkali Mataev[1,*]

Abstract

This study investigates the synthesis and structural characterization of the polycrystalline nanocomposite material ytterbium manganate-cobalt chromite ($YbMnO_3$-$CoCr_2O_4$). The synthesis was performed using the sol-gel and Pechini methods. X-ray diffraction (XRD) analysis was used to determine the phase composition, revealing the presence of perovskite-type ytterbium manganate and spinel-type cobalt chromite. Data analysis was conducted using the powder diffraction x-ray line (PDXL) program, confirming that the nanocomposite is a two-phase system consisting of orthorhombic perovskite and cubic spinel phases. Morphological analysis was carried out using scanning electron microscopy (SEM) and high-resolution transmission electron microscopy (TEM) to confirm the elemental composition and provide average particle size measurements and their distribution. The particle sizes were determined to be 215-525 nm for $YbMnO_3$ and 2.11-3.19 µm for $CoCr_2O_4$. Additionally, 3D surface profiles and nanomaterial growth measurements were obtained using the MP-45030TDI 3D modeling software. This synthesized nanocomposite is significant for spintronic devices and multifunctional sensors.

Keywords: Polycrystalline nanocomposites; Orthorhombic; Perovskite-type ytterbium manganate.
Received: 17 September 2024; Revised: 01 November 2024; Accepted: 02 November 2024.
Article type: Research article.

1. Introduction

Perovskite compounds with the chemical formula ABO_3 form a large class of materials known for their wide-ranging functionalities.[1,2] Typical examples include ferroelectric compounds such as $BaTiO_3$ and $PbTiO_3$, as well as those exhibiting colossal magnetoresistance, like $La_{1-x}Ba_xMnO_3$. These materials are commonly used in applications such as converters, actuators, capacitors, memory devices, and magnetic sensors. Manganite-based perovskites have garnered significant attention due to their quantum phenomena, driven by the strong interactions between charge, spin, and orbital degrees of freedom. This has led to extensive experimental and theoretical investigations into nearly all rare-earth-based compounds' structural, electronic, and magnetic properties.[1,2]

Rare-earth manganites stand out for their extraordinary properties, including thermal and chemical stability, supermagnetism, superconductivity, supercapacitance, photocatalytic activity, thermoelectric efficiency, and dielectric behavior.[3,4] Depending on the ionic radius of the rare-earth element, manganite-based perovskites can exist in either an orthorhombic phase (o-$RMnO_3$, space group Pbnm) or a hexagonal phase (h-$RMnO_3$, space group P63cm).[5] The general formula for these compounds, $RMnO_3$ (where R represents a rare-earth cation), accommodates two crystal symmetries, both of which have attracted considerable attention due to their fundamental scientific interest and practical potential. The hexagonal structure with space group P63cm is the most stable crystalline phase for small-radius cations like Yb. Recently, perovskites have received increased attention for their robust structure, thermal stability, catalytic properties, and significant role in energy applications such as solid fuels and solar cells.[6-9] Supercapacitance has also become a crucial concept in the study of manganite perovskites, with $YbMnO_3$ emerging as a promising material due to its desirable supercapacitive properties. Supercapacitors are favored among energy storage devices for

[1] *Department of Chemistry, Faculty of Natural Sciences, Kazakh National Women's Teacher Training University, Almaty, 050000, Kazakhstan*
[2] *Institute of Engineering Physics and Radioelectronics, Siberian Federal University, Krasnoyarsk, 660041, Russia*
**Email:* mataev_06@mail.ru (M. Mataev);
zhaisanbayeva.moldir@gmail.com (M. Zhaisanbayeva)

their higher energy storage efficiency than traditional batteries.[10]

Transition metal spinel structures, characterized by the general formula XY_2O_4, have similarly attracted significant interest due to their intriguing properties, including colossal magnetoresistance (CMR), dielectric anomalies, and ferroelectric behavior.[11-13] The spinel family, represented by $ACr_3^{2+}X_4$ (where A^{2+} = Mn, Zn, Cd, Hg and X^{2-} = O, S, Se), has been extensively studied because of the close correlation between their structural, electronic, and magnetic properties.[14-16] Magnetism in spinels arises from the partially filled d-orbitals in transition metals.[17] Cobalt chromites ($CoCr_2O_4$), in particular, exhibit spontaneous magnetization, spin-induced electrical polarization, and outstanding physical properties.[18,19] In $CoCr_2O_4$, magnetic Co^{2+} ions ($3d^7$, s = 3/2) occupy tetrahedral X-sites, while magnetic Cr^{3+} ions ($3d^3$, s = 3/2) are positioned in octahedral Y-sites.[20,21] This creates a strong X-site preference for Co^{2+}, strengthening the Y–Y interactions. Cobalt chromites are known for their long-range ferrimagnetic order, which occurs at a temperature of approximately 94 K.[21,22] In contrast, the X–Y interaction in $CoFe_2O_4$ (cobalt ferrites) is stronger due to the compound's inverse spinel structure.

When Fe^{3+} ions replace Cr^{3+} ions in the $CoCr_2O_4$ lattice, some Fe atoms move into tetrahedral positions, causing Co^{2+} ions at X-sites to shift towards octahedral regions. This substitution alters the electronic and magnetic properties of $CoCr_2O_4$, resulting in a partial inverse spinel structure. Consequently, the occupation of Co^{2+} and Fe^{3+} ions at different sites affects the transition temperature, particle size, cationic charge, magnetic coupling, and electronic states. Since the spin states of atoms in other regions vary, the total magnetic moment changes accordingly.[21-26]

Due to their fascinating physical properties, chromite spinels are used in multiferroic memory devices,[27] microwave absorbers,[28] disk recording media,[29] electrical devices,[30] heat-resistant pigments,[31] gas-sensitive materials,[32] and as photocatalysts for hydrogen production and pollutant degradation.[33] This study presents the synthesis of chromite-manganite nanocomposites through the sol-gel method. X-ray diffraction analysis confirmed the formation of both single-phase,[34] two-phase composite nanomaterials. Additionally, thermal, microstructural, optical, magnetic,[35] and magnetocaloric properties of chromite spinel $Ni_{0.5}Mn_{0.5}Cr_2O_4$, synthesized by the sol-gel method, were investigated.[36] More detailed information on the synthesis of magnetization of composites and the application of potential polymer materials is presented in the papers.[37-39]

In this project, we synthesized this nanocompound for the first time via electrochemical deposition, demonstrating its potential as a high-performance supercapacitor and a viable candidate for lithium-ion batteries. A manganite-spinel double nanocomposite with advanced functional applications was synthesized using sol-gel and Pechini methods. The resulting material was characterized through qualitative and quantitative techniques.

2. Experimental

2.1 Materials and reagents

The reagents ytterbium (III) oxide (Yb_2O_3), manganese (III) oxide (Mn_2O_3), chromic oxide (Cr_2O_3), and cobalt carbonate ($CoCO_3$) were purchased from Darmstadt (Germany) and were of analytical grade and used without further purification or treatment. The experiment used citric acid and ethylene glycol purchased from Sigma-Aldrich (Germany), which were used as received. All grinding was done using an agate mortar from Sigma-Aldrich (Germany). Deionized (DI) water used in this experiment was collected from Puris' reverse osmosis system (Puris Eco 1600-M, South Korea).

2.2 Synthesis of $YbMnO_3$-$CoCr_2O_4$ composite nanomaterial

The two-phase nanomaterial $YbMnO_3$-$CoCr_2O_4$ was synthesized using sol-gel and Pechini methods.[40] To obtain a double composite, 0.5 g of the initial metal oxides are carefully mixed where the metal oxides are doped with 0.2 g of cobalt carbonate. The mixture was thoroughly ground in an agate mortar and dissolved in 10 mL DI water. 0.5 g of citric acid and 2 mL of ethylene glycol (gelling agent) are added, which promotes the formation of a homogeneous phase in the samples. The mixture is heated in an electric furnace at 70 °C until a gel is obtained. The resulting viscous gel is processed in a muffle furnace at a temperature of 600 °C for 35 minutes. After converting the composition into powder, it was fired at increasing temperatures of 700-1100 °C. The firing was divided into five stages, totaling 39 h. The result obtained from this work was labelled as the synthesised multifunctional two-phase perovskite-spinel nanocomposite and well preserved for characterization and further analysis.

2.3 Characterization

The phase composition of the as-synthesized perovskite nanocomposite was measured using a Miniflex 600 RIGAKU X-ray diffractometer (Japan) with an SC-70 detector. A 3-90 ° scanning range was selected at 40 kV and 15 mA at a diffraction angle of 2θ and a 2 °/min scanning speed. A JSM-6510LV JEOL scanning electron microscope (Japan) running at 5 to 20 kV was used to measure the morphological features of the as-prepared nanocomposite. Data processing and calculations were done using PDXL and MP-45030TDI 3D modeling programs. A high-resolution transmission electron microscopy (HR-TEM) analysis was carried out using JEM2100 LaB6 (JEOL, Japan) and operated at 80 kV to study

the distribution of nanoparticles within the structure of the synthesized composite material.

3. Results and discussion

Analyzing the perovskite nanomanganite's structure through X-ray diffraction (XRD) allowed for determining its phase composition. The distinct characteristic peaks corresponding to $CoCr_2O_4$ and $YbMnO_3$ phases confirm the successful formation of the perovskite composite. The well-defined, sharp peaks observed in the diffraction patterns indicate the crystallinity of the synthesized material. As shown in Fig. 1, the XRD analysis of the calcined polycrystalline samples reveals the presence of two main composites: hexagonal ytterbium manganate ($YbMnO_3$) and spinel cobalt chromite ($CoCr_2O_4$), a multiferroic phase. Prominent peaks corresponding to the Miller indices (111), (220), (311), (222), (400), (422), (511), and (533) are attributed to the $CoCr_2O_4$ cubic phase, which is in close agreement with previous literature.[41] The diffraction peaks associated with $YbMnO_3$ are broader compared to $CoCr_2O_4$, indicating the formation of smaller crystallites.[42]

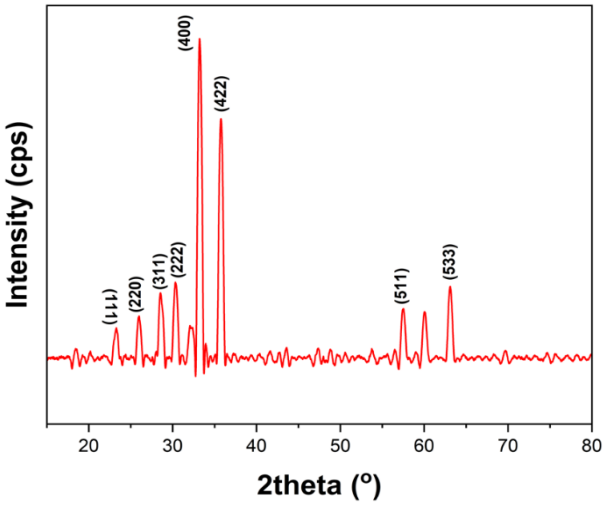

Fig. 1: XRD of $YbMnO_3$-$CoCr_2O_4$ nanoparticles.

Fig. 2 presents the quantitative analysis of the as-prepared composite material. The results, along with the calibration data, indicate that the percentage composition is 47% ytterbium manganate ($YbMnO_3$) and 53% cobalt chromite ($CoCr_2O_4$) (Table 2).

Table 1: Quantitative analysis of the composite material.

Phase name	Formula	Content (%)
Perovskite	$YbMnO_3$	47
Cochromite	$CoCr_2O_4$	53

According to X-ray phase analysis, the perovskite phase of the nanocomposite is $YbMnO_3$. The composition of multiferroics has an orthorhombic syngony with a primitive lattice type. The spinel phase is $CoCr_2O_4$ with a cubic crystal structure (Table 2).

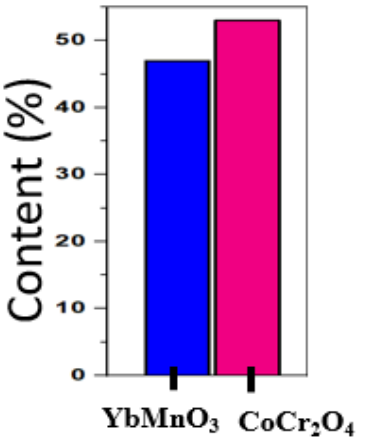

Fig. 2: Quantitative analysis results.

The samples' average crystallite size and lattice strain were studied using the Williamson-Hall analysis. In this study, we analyzed the diffraction profile of the lines via the Williamson-Hall method. Fig. 1 was used to calculate the full width at half maximum (FWHM) of (β_{hkl}), and then (β_{hkl}) and 2θ were used to determine $\beta_{hkl}\cos\theta$ and $4\sin\theta$ for each peak of the $YbMnO_3$-$CoCr_2O_4$ nanoparticles. The Williamson-Hall plot was employed to calculate the crystallite size P and intrinsic lattice strain using Eq. (1):

$$\beta_{hkl}\cos\theta = \frac{K\lambda}{P} + 1e\sin\theta \quad (1)$$

where P is the crystallite size and e is the lattice strain.

The crystallite size of $YbMnO_3$ was 77 nm, and that of $CoCr_2O_4$ was 210.6 nm, based on the y-intercepts of the best-fit line. These values differ significantly from the crystallite sizes observed via scanning electron microscope (SEM) (discussed below), as the Williamson-Hall method involves several assumptions. Additionally, it was noted that the model exhibits a positive slope, which indicates the presence of defects, such as point defects, line defects, and surface and volume defects within the crystal. These deviations from perfect crystallinity led to a broadening of the diffraction peaks.[43,44]

As seen in Fig. 3, several reflection points lie above the line of best fit, suggesting that the powder crystallites are thinnest in the <100> direction. The intrinsic strain values of 10 and 2 were respectively calculated for $YbMnO_3$ and $CoCr_2O_4$ from the slope of Eq. (1). The positive intrinsic strain values indicate that the synthesized crystals are under tensile stress rather than compressive strain.[43,44]

The surface and textual morphology of the nanocomposite was studied using SEM (JSM-6510LV JEOL), and their spectrum is shown in Fig. 4 above. The synthesized $YbMnO_3$ perovskite, which could be seen as orthorhombic, from Fig. 4 (A and B), has a structural crystal size from 215 to 525 nm, and the $CoCr_2O_4$ spinel, which appears to be cubic, has a microstructural phase size from 2.11 to 3.19 µm. The energy-dispersive x-ray spectroscopy (EDX) spectrum also confirms

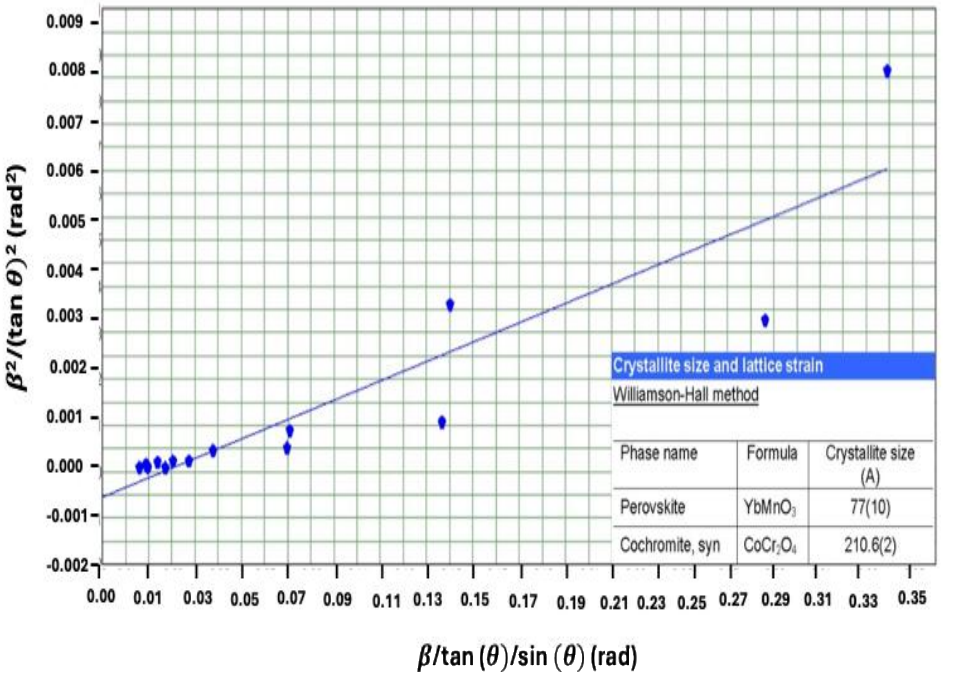

Fig. 3: Williamson-Hall plot of $\beta_{hkl}\cos\theta$ vs $4\sin\theta$ $YbMnO_3$-$CoCr_2O_4$ nanoparticles.

Table 2: Result of quantitative analysis of the crystal lattice.

Phase formula	Types of syngony	a, Å	b, Å	c, Å	V, Å^3	Space group	Z	Theor. density (g/cm^3)
$YbMnO_3$	orthorhombic	5.323(3)	5.579(3)	7.584(4)	225.2(2)	Pbnm (62)	4	7.890
$CoCr_2O_4$	cubic	8.3360(18)	8.3360(18)	8.3360(18)	579.3(2)	$Fd\bar{3}m$ (227)	8	5.164

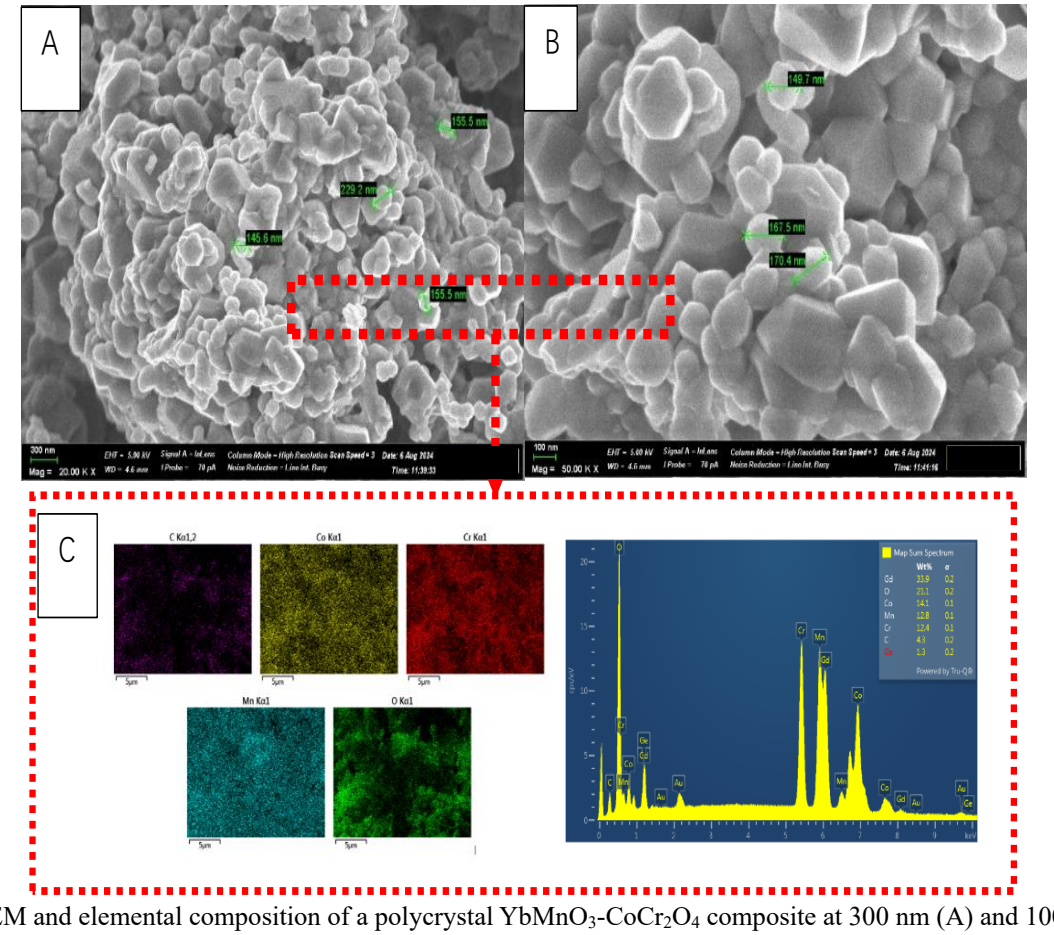

Fig. 4: SEM and elemental composition of a polycrystal $YbMnO_3$-$CoCr_2O_4$ composite at 300 nm (A) and 100 nm (B).

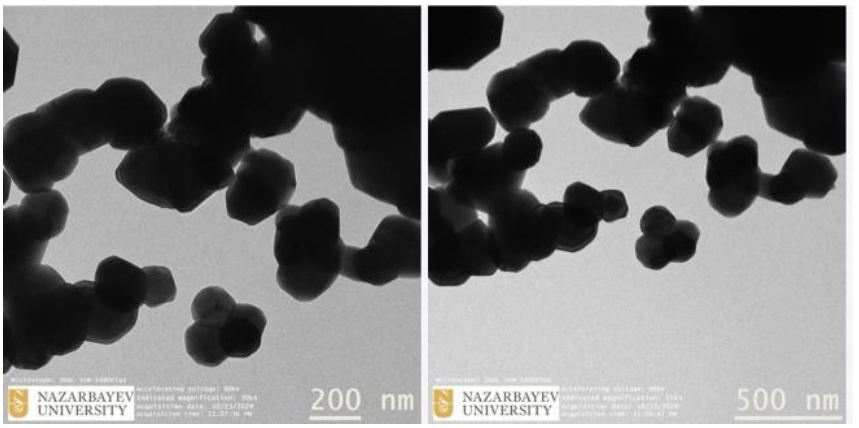

Fig. 5: TEM image of polycrystal $YbMnO_3$-$CoCr_2O_4$ composite at 200 and 500 nm.

the presence and proportions of the masses of elements in a two-phase nanomaterial (Yb, Cr, Co, and Mn), confirming the correspondence of the elemental composition map to theoretical data (Fig. 4C). Other trace elements such as Au and Ge observed in the spectrum could result from other external sources, including sample holders among others.

To analyze the size and shape of the polycrystal $YbMnO_3$-$CoCr_2O_4$ composite nanoparticles, TEM was used, and the results are presented in Fig. 5. The image shows that the nanoparticles are well-dispersed and exhibit a spherical shape. Additionally, they display some degree of agglomeration and appear larger than the average crystallite size obtained from the XRD. The presence of agglomeration between nanoparticles could possibly result from magnetic interactions, as reported in the literature.[45]

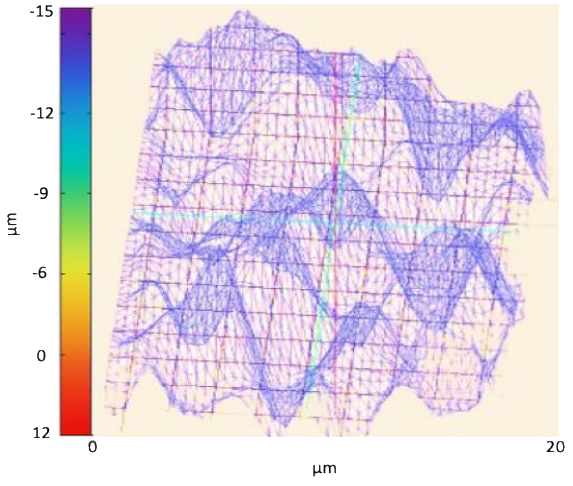

Fig. 6: $YbMnO_3$-$CoCr_2O_4$ - 3D surface reconstruction.

MP-45030TDI 3D modeling software was used to analyze the surface reconstruction of the synthesized $YbMnO_3$-$CoCr_2O_4$. Contour mapping, utilizing SEM, provided solutions for the analysis and visualization of 3D mapping, anaglyph images, profiles, and the measurement of nanomaterial growth, as shown in Fig. 6. The SEM images also offered a deeper understanding of the complex microstructures. This 3D imaging technique enables intuitive calculation of surface characteristics. From the results, the height of the studied microstructure was measured at 20 µm, with a horizontal depth of 24 µm, and a metrological surface width of 20 µm. These structural analysis results expand the database of nanocomposite materials with promising electrophysical properties.

4. Conclusion

The resulting two-phase nanomaterial's phase structure and elemental composition were analyzed. The crystallographic results confirmed that $YbMnO_3$, a syngonal type of two-phase polycrystal, exhibits an orthorhombic structure. With the number of formula units (Z) of iron manganite equal to 4, the shape parameters of the orthorhombic unit cell were determined as a = 5.323 Å, b = 5.579 Å, and c = 7.584 Å. For $CoCr_2O_4$, which has 8 formula units (Z = 8), the cubic unit cell dimensions were found to be a = b = c = 8.3360 Å. Additionally, the formation of the product was confirmed through nanoscale and elemental composition analysis. Table 1 presents the relevant data, showing that the $YbMnO_3$ phase (Z = 4) crystallizes in an orthorhombic lattice with the space group Pbnm. The $CoCr_2O_4$ phase (Z = 8), in contrast, crystallizes in a cubic lattice with the space group $Fd\bar{3}m$. The as-prepared YbMnO3-CoCr2O4 nanocomposite, combining ferromagnetic and mutiferroic phases holds ample potential for application in multifunctional devices such as spintronic components, energy harvesting, and magnetoelectric sensors where a fabrication between electric and magnetic properties is crucial for performance improvement.

Conflict of Interest

There is no conflict of interest.

Supporting Information

Not applicable.

References

[1] M. Dawber, K. M. Rabe, J. F. Scott, Physics of thin-film ferroelectric oxides, *Reviews of Modern Physics*, 2005, **77**, 1083-1130, doi: 10.1103/revmodphys.77.1083.

[2] J. Hu, G. Li, X. Huang, W. Zhang, Role of the crystal electric

field on the two magnetic transitions in the orthorhombic $YbMnO_3$ perovskite, *Physical Review B*, 2019, **99**, 134418, doi: 10.1103/physrevb.99.134418.
[3] Y. Liu, Z. Wang, J. M. Veder, Z. Xu, Y. Zhong, W. Zhou, M. O. Tade, S. Wang, Z. Shao, Highly defective layered double perovskite oxide for efficient energy storage via reversible pseudocapacitive oxygen-anion intercalation, *Advanced Energy Materials*, 2018, **8**, 1702604, doi: 10.1002/aenm.201702604.
[4] R. Dhinesh Kumar, R. Jayavel, Hydrothermal synthesis and magnetic property studies of multiferroic $YMnO_3$ nanorods, *Advanced Materials Research*, 2012, **584**, 253-257, doi: 10.4028/www.scientific.net/amr.584.253.
[5] Y. H. Huang, H. Fjellvåg, M. Karppinen, B. C. Hauback, H. Yamauchi, J. B. Goodenough, Crystal and magnetic structure of the orthorhombic perovskite $YbMnO_3$, *Chemistry of Materials*, 2006, **18**, 2130-2134, doi: 10.1021/cm052758t.
[6] J. Liu, C. Toulouse, P. Rovillain, M. Cazayous, Y. Gallais, M.-A. Measson, N. Lee, S. W. Cheong, A. Sacuto, Lattice and spin excitations in multiferroic h-$YbMnO_3$, *Physical Review B*, 2012, **86**, 184410, doi: 10.1103/physrevb.86.184410.
[7] B. Zhu, Y. Huang, L. Fan, Y. Ma, B. Wang, C. Xia, M. Afzal, B. Zhang, W. Dong, H. Wang, P. D. Lund, Novel fuel cell with nanocomposite functional layer designed by perovskite solar cell principle, *Nano Energy*, 2016, **19**, 156-164, doi: 10.1016/j.nanoen.2015.11.015.
[8] H. Mohammad Shiri, A. Ehsani, Electrosynthesis of neodymium oxide nanorods and its nanocomposite with conjugated conductive polymer as a hybrid electrode material for highly capacitive pseudocapacitors, *Journal of Colloid and Interface Science*, 2017, **495**, 102-110, doi: 10.1016/j.jcis.2017.01.097.
[9] S. Gowreesan, A. Ruban Kumar, Structural, magnetic, and electrical property of nanocrystalline perovskite structure of iron manganite ($FeMnO_3$), *Applied Physics A*, 2017, **123**, 689, doi: 10.1007/s00339-017-1302-x.
[10] H. Wu, X. Zhu, Perovskite oxide nanocrystals: synthesis, characterization, functionalization, and novel applications, Perovskite Materials - Synthesis, Characterisation, Properties, and Applications, InTech, 2016, ISBN: 978-953-51-2245-6.
[11] D. P. Dutta, J. Manjanna, A. K. Tyagi, Magnetic properties of sonochemically synthesized $CoCr_2O_4$ nanoparticles, *Journal of Applied Physics*, 2009, **106**, 043915, doi: 10.1063/1.3204659.
[12] K. Singh, A. Maignan, C. Simon, C. Martin, $FeCr_2O_4$ and $CoCr_2O_4$ spinels: Multiferroicity in the collinear magnetic state?, *Applied Physics Letters*, 2011, **99**, 172903, doi: 10.1063/1.3656711.
[13] W. Kleemann and C. Binek, Multiferroic and Magnetoelectric Materials, *Springer Tracts in Modern Physics*, 2013, **246**, 163-187, doi: 10.1007/978-3-642-32042-2_5.
[14] S. Weber, P. Lunkenheimer, R. Fichtl, J. Hemberger, V. Tsurkan, A. Loidl, Colossal magnetocapacitance and colossal magnetoresistance in $HgCr_2S_4$, *Physical Review Letters*, 2006, **96**, 157202, doi: 10.1103/physrevlett.96.157202.
[15] Y. Yamasaki, S. Miyasaka, Y. Kaneko, J. P. He, T. Arima, Y. Tokura, Magnetic reversal of the ferroelectric polarization in a multiferroic spinel oxide, *Physical Review Letters*, 2006, **96**, 207204, doi: 10.1103/physrevlett.96.207204.
[16] K. Dey, S. Majumdar, S. Giri, Ferroelectricity in spiral short-range-ordered magnetic state of spinel $MnCr_2O_4$: Significance of topological frustration and magnetoelastic coupling, *Physical Review B*, 2014, **90**, 184424, doi: 10.1103/physrevb.90.184424.
[17] N. A. Hill, Why are there so few magnetic ferroelectrics?, *The Journal of Physical Chemistry B*, 2000, **104**, 6694-6709, doi: 10.1021/jp000114x.
[18] Z. Tian, C. Zhu, J. Wang, Z. Xia, Y. Liu, S. Yuan, Size dependence of structure and magnetic properties of $CoCr_2O_4$ nanoparticles synthesized by hydrothermal technique, *Journal of Magnetism and Magnetic Materials*, 2015, **377**, 176-182, doi: 10.1016/j.jmmm.2014.10.090.
[19] M. Akyol, İ. Adanur, A. O. Ayaş, A. Ekicibil, Magnetic field dependence of magnetic coupling in $CoCr_2O_4$ nanoparticles, *Physica B: Condensed Matter*, 2017, **525**, 144-148, doi: 10.1016/j.physb.2017.09.021.
[20] K. Tomiyasu, J. Fukunaga, H. Suzuki, Magnetic short-range order and reentrant-spin-glass-like behavior in $CoCr_2O_4$ and $MnCr_2O_4$ by means of neutron scattering and magnetization measurements, *Physical Review B*, 2004, **70**, 214434, doi: 10.1103/physrevb.70.214434.
[21] C. L. Li, T. Y. Yan, G. O. Barasa, Y. H. Li, R. Zhang, Q. S. Fu, X. H. Chen, S. L. Yuan, Negative magnetization and exchange bias effect in Fe-doped $CoCr_2O_4$, *Ceramics International*, 2018, **44**, 15446-15452, doi: 10.1016/j.ceramint.2018.05.200.
[22] I. Efthimiopoulos, Z. T. Y. Liu, S. V. Khare, P. Sarin, T. Lochbiler, V. Tsurkan, A. Loidl, D. Popov, Y. Wang, Pressure-induced transition in the multiferroic $CoCr_2O_4$ spinel, *Physical Review B*, 2015, **92**, 064108, doi: 10.1103/physrevb.92.064108.
[23] H. Zhang, W. Wang, E. Liu, X. Tang, G. Li, H. Zhang, G. Wu, Compensation effect and magnetostriction in $CoCr_2$-$xFexO_4$, *Physica Status Solidi (b)*, 2013, **250**, 1287-1292, doi: 10.1002/pssb.201248470.
[24] A. Dashora, M. Suthar, K. Kumar, R. J. Choudhary, D. M. Phase, H. Sakurai, N. Tsuji, Y. Sakurai, B. L. Ahuja, Study of magnetism in Fe doped $CoCr_2O_4$ using magnetic Compton scattering and first-principles computations, *Journal of Alloys and Compounds*, 2020, **824**, 153883, doi: 10.1016/j.jallcom.2020.153883.
[25] S. Ganguly, R. Chimata, B. Sanyal, Overcoming magnetic frustration and promoting half-metallicity in spinel $CoCr_2O_4$ by doping with Fe, *Physical Review B*, 2015, **92**, 224417, doi: 10.1103/physrevb.92.224417.
[26] M. Ptak, M. Mączka, A. Pikul, P. E. Tomaszewski, J. Hanuza, Magnetic and low temperature phonon studies of $CoCr_2O_4$ powders doped with Fe(III) and Ni(II) ions, *Journal of Solid State Chemistry*, 2014, **212**, 218-226, doi: 10.1016/j.jssc.2013.10.048.
[27] J. F. Scott, Multiferroic memories, *Nature Materials*, 2007, **6**, 256-257, doi: 10.1038/nmat1868.
[28] Z. H. Shah, S. Riaz, S. Atiq, S. Naseem, Tunable structural and electrical impedance properties of ordered and disordered iron oxide phases for capacitive applications, *Ceramics International*, 2018, **44**, 16352-16364, doi:

10.1016/j.ceramint.2018.06.043.
[29] W. Kleemann, Multiferroic and magnetoelectric nanocomposites for data processing, *Journal of Physics D: Applied Physics*, 2017, **50**, 223001, doi: 10.1088/1361-6463/aa6c04.
[30] Z. Chu, M. PourhosseiniAsl, S. Dong, Review of multi-layered magnetoelectric composite materials and devices applications, *Journal of Physics D: Applied Physics*, 2018, **51**, 243001, doi: 10.1088/1361-6463/aac29b.
[31] A. L. Fernández, L. de Pablo, Formation and the colour development in cobalt spinel pigments, *Pigment & Resin Technology*, 2002, **31**, 350-356, doi: 10.1108/03699420210449043.
[32] X. Niu, W. Du, W. Du, Preparation and gas sensing properties of ZnM_2O_4 (M = Fe, co, Cr), *Sensors and Actuators B: Chemical*, 2004, **99**, 405-409, doi: 10.1016/j.snb.2003.12.007.
[33] S. Boumaza, R. Bouarab, M. Trari, A. Bouguelia, Hydrogen photo-evolution over the spinel $CuCr_2O_4$, *Energy Conversion and Management*, 2009, **50**, 62-68, doi: 10.1016/j.enconman.2008.08.027.
[34] W. Wang, J. Li, P. Ni, B. Liu, Q. Chen, Y. Lu, H. Wu, B. Cao, Z. Liu, Improved synthesis of perovskite $CsPbX_3@SiO_2$ (X = Cl, Br, and I) quantum dots with enhanced stability and excellent optical properties, *ES Materials & Manufacturing*, 2019, **4**, 66-73, doi: 10.30919/esmm5f219.
[35] S. B. Jathar, S. R. Rondiya, B. R. Bade, M. P. Nasane, S. V. Barma, Y. A. Jadhav, A. V. Rokade, K. B. Kore, D. S. Nilegave, P. U. Tandale, S. R. Jadkar, A. M. Funde, Facile method for synthesis of CsPbBr3 perovskite at room temperature for solar cell applications, *ES Materials & Manufacturing*, 2021, **12**, 72-77, doi: 10.30919/esmm5f1036.
[36] F. Hcini, S. Hcini, M. M. Almoneef, M. H. Dhaou, M. S. Alshammari, A. Mallah, S. Zemni, N. Lefi, M. L. Bouazizi, Thermal, microstructural, optical, magnetic and magnetocaloric studies for $Ni0.5Mn0.5Cr_2O_4$ chromite spinel prepared using Sol-gel method, *Journal of Molecular Structure*, 2021, **1243**, 130769, doi: 10.1016/j.molstruc.2021.130769.
[37] G. S. Patrin, M. M. Mataev, M. R. Abdraimova, Z. I. Tursinova, A. T. Kezdikbaeva, Y. G. Shiyan, V. G. Plekhanov, Magnetic properties of the $DyMn_2O_5$-Mn_3O_4 nanoparticle composite, *Technical Physics*, 2021, **66**, 635-641, doi: 10.1134/s1063784221040137.
[38] U. Nakan, S. Bieerkehazhi, B. Tolkyn, G. A. Mun, M. Assanov, M. E. Nursultanov, R. K. Rakhmetullayeva, K. Toshtay, E.-S. Negim, A. Ydyrys, Synthesis, characterization and antibacterial application of copolymers based on N, N-dimethyl acrylamide and acrylic acid, *Materials*, 2021, **14**, 6191, doi: 10.3390/ma14206191.
[39] S. Turganbay, S. B. Aidarova, N. E. Bekturganova, C. S. Li, K. B. Musabekov, S. S. Kumargalieva, K. Toshtay, Nanoparticles of sulfur as fungicidal products for agriculture, *Eurasian Chemico-Technological Journal*, 2012, **14**, 313-319, doi: 10.18321/ectj128.
[40] S. A. Ehsanizadeh, A. S. Abbas, F. S. Razavi, E. A. Dawi, A. M. M. Ibrahim, M. Salavati-Niasari, Facile synthesis and characterization of $SrMnO_3/SrCO_3$ nanocomposites by Pechini Sol-gel method as efficient and innovated active materials for electrochemical hydrogen storage application, *International Journal of Hydrogen Energy*, 2024, **60**, 392-401, doi: 10.1016/j.ijhydene.2024.02.219.
[41] J. K. Galivarapu, D. Kumar, A. Banerjee, V. Sathe, G. Aquilanti, C. Rath, Effect of size reduction on cation distribution and magnetic transitions in $CoCr_2O_4$ multiferroic: EXAFS, magnetic and diffused neutron scattering measurements, *RSC Advances*, 2016, **6**, 63809-63819, doi: 10.1039/c6ra10189e.
[42] R. Das, P. Poddar, Ionic control on the morphology of ytterbium manganese oxide nanorods and nanoplates in a surfactant-free synthesis and their magnetic properties, *The Journal of Physical Chemistry C*, 2014, **118**, 13268-13275, doi: 10.1021/jp503591f.
[43] Y. T. Prabhu, K. V. Rao, V. S. S. Kumar, B. S. Kumari, X-ray analysis by williamson-hall and size-strain plot methods of ZnO nanoparticles with fuel variation, *World Journal of Nano Science and Engineering*, 2014, **4**, 21-28, doi: 10.4236/wjnse.2014.41004.
[44] M. Rabiei, A. Palevicius, A. Dashti, S. Nasiri, A. Monshi, A. Doustmohammadi, A. Vilkauskas, G. Janusas, X-ray diffraction analysis and williamson-hall method in USDM model for estimating more accurate values of stress-strain of unit cell and super cells (2 × 2 × 2) of hydroxyapatite, confirmed by ultrasonic pulse-echo test, *Materials*, 2021, **14**, 2949, doi: 10.3390/ma14112949.
[45] K. Nadeem, H. U. Rehman, F. Zeb, A. E., M. Kamran, N. A. Noshahi, H. Abbas, Magnetic phase diagram and dielectric properties of Mn doped $CoCr_2O_4$ nanoparticles, *Journal of Alloys and Compounds*, 2020, **832**, 155031, doi: 10.1016/j.jallcom.2020.155031.